Ngo, Q. M., Ho, Y. L. D., Pugh, J. R., Sarua, A., & Cryan, M. J. (2018). Enhanced UV/blue fluorescent sensing using metal-dielectric-metal aperture nanoantenna arrays. *Current Applied Physics*, *18*(7), 793-798. https://doi.org/10.1016/j.cap.2018.04.007

Highlight - 2nd REVISION

Enhanced UV/Blue Fluorescent Sensing Using Metal-Dielectric-Metal Aperture Nanoantenna Arrays

*Quang Minh Ngo[1,2], Ying-Lung D. Ho[1], Jon R. Pugh[1], Andrei Sarua[3] and Martin J. Cryan[1]**

[1]Department of Electrical and Electronic Engineering, University of Bristol, Bristol BS8 1UB, United Kingdom

[2]Institute of Materials Science, Vietnam Academy of Science and Technology, 18 Hoang Quoc Viet, Cau Giay, Hanoi, Vietnam

[3]H. H. Wills Physics Laboratory, School of Physics, University of Bristol, Bristol BS8 1TL, United Kingdom

**Corresponding author: m.cryan@bristol.ac.uk*

Abstract: Subwavelength aperture antenna arrays are designed and fabricated for potential applications in fluorescence sensing in the near UV/blue range. They are designed using finite-difference time-domain (FDTD) simulation, fabricated using focused ion beam etching and characterised using angular Fourier spectroscopy. The aperture arrays are formed in the top layer of an aluminum-silica-aluminum trilayer and produce a maximum simulated field intensity enhancement of 5.8 times at 406nm and highly directive emission with a beamwidth of 8.3 deg. The normal incidence reflection response has been measured and shows reasonable agreement with modelled results. In addition, to investigate higher field intensity enhancements, bowtie aperture arrays are simulated and the influence of parameters such as dielectric gap, position of dipole source, and aperture shape and size are discussed and show enhancements up to 67 times are possible.

Key words: nanoantennas, aperture arrays, plasmonics.

1. INTRODUCTION

The concept of surface plasmons or plasmonics has seen widespread use in implementing optical devices and photonic circuits [1-3] as well as in chemical sensing technologies [4-8]. Recent advances in metallic nanoparticle synthesis and nanofabrication methods have led to a variety of new nanostructures composed of nanoparticles, nanoholes, and other structures with precisely controlled shapes, sizes, and/or spacers, with novel physical and chemical properties [9-12]. Such exquisite fabrication and synthesis control in combination with advances in theory and the emergence of quantitative electromagnetic simulation tools has provided a better understanding of the optical properties of single and coupled metallic nanostructures of various sizes and shapes [10,11]. Various approaches for modifying metallic surfaces and structures make it possible to effect the selective binding and

detection of specific targets for chemical and biological sensing. Recently metallic nanoparticles and nanoantenna arrays have been used because of their ability to greatly enhance local electromagnetic fields and confinement [13-17]. Specifically it was demonstrated that metal-dielectric-metal (MDM) structures of nanoantennas are a very effective alternative to increase the performance of nanoantennas for chemical and biological [15,16] and humidity [17] sensing applications. Nanoantennas are also very suitable for biological applications because they are able to track emission from fluorescent makers in cells with sub-diffraction limited resolution, as well as the destruction of cancer cells using the heating of resonant nanoparticles [18,19].

In 1998, Ebbesen *et al.* demonstrated the extraordinary optical transmission through the subwavelength hole arrays perforated in a gold or silver film which is generally attributed to the resonant excitation of surface plasmons [20]. Subsequent work [21] confirmed that surface plasmons formed on both sides of the metallic surface resonantly couple through the subwavelength hole arrays, which enhances the light transmission for specific wavelengths depending on the lattice constant of the hole arrays and the dielectric constants of the metallic and the surrounding media. This structure has shown potential for surface plasmon resonance sensing, since they can couple incident light directly into surface plasmons. The feasibility of using subwavelength hole arrays for biosensing where a spectral shift is observed after the immobilization of molecules on metallic film using a broadband source and a spectrometer has also been shown previously [22-24]. In the context of fluorescent biosensing applications, plasmonic nanoantennas can create highly enhanced local fields when pumped resonantly, and through Purcell enhancement can significantly enhance fluorescent emission, both of which can improve fluorescence based sensors [25-27]. Recently we have shown fluorescent emission enhancement using aluminium nanoantenna arrays in the near-UV [10]. Scanning confocal photoluminescence measurements of the arrays showed up to 1.9 times more enhancement of the fluorescent signal compared to a reference on glass. The simulations and measurements showed strong dependence of the emission on angle, with maximum emission at high angles with respect to the normal, so that a high numerical aperture (NA) is necessary to collect the emission. In this work, aperture arrays in a MDM structure are considered as another choice which give high field enhancement and strong normal emission enabling straightforward collection of fluorescence. This is an extension of a single metal layer aperture array, with the addition of a lower metal layer which prevents downward emission of fluorescence, further enhancing upward emission.

The structure consists of a subwavelength aperture array which is Focused Ion Beam (FIB) etched into the upper aluminium layer of the MDM structure. We fabricated a 14 by 14 element array and performed angle resolved reflectance measurements. We simulated the enhancement with the FDTD method using electric dipoles placed inside the subwavelength aperture arrays. The simulated enhancement definition here is a very simple one which is the ratio of total emitted power from a dipole with and without the antenna which does not account for the very strong focusing effects that occur due the periodic nature of the array [10]. In addition, we study the influence of antenna parameters such as silica gap thickness, aperture size and shape, and also position of the electric dipole sources on the fluorescent enhancement. The paper is composed of three sections. The first section introduces the

design and fabrication of subwavelength aperture antennas. The second section presents the results and discussion. In the final section, we present the conclusions.

2. DESIGN AND FABRICATION

A. Simulated reflection spectra

Our study uses a silicon substrate covered by a 100 nm thick aluminium (Al) layer, which is thick enough to prevent optical transmission into the silicon, further capped by a continuous silica (SiO_2) film of thickness *d*. The nanoantenna structure is formed by a square lattice (lattice constant L = 350 nm) of subwavelength square apertures (width, w = 175 nm) perforated through an Al layer (thickness t) on top of the SiO_2 film, as illustrated in Fig. 1(a). The simulations were performed using a commercial 3D full-wave electromagnetic wave solver Lumerical FDTD [28]. To calculate the reflectance spectra of the nanoantenna structure, perfectly matched absorbing boundary conditions are used at the top and the bottom boundaries [29]. In the lateral direction, periodic boundary conditions are applied. Incident light to the unit cell was a plane wave. The reflectance was collected with a power monitor placed behind the radiation source. Fig. 1(b) shows the reflectance spectra of the normally incident wave (θ_i = 0°) for several SiO_2 inter-layer thicknesses (d) and upper layer thicknesses (t). As shown in Fig. 1(b), the reflectance spectrum shows two dips for each structure. The dip at longer wavelengths, above 480nm with quality factor (Q-factor) of ~ 8.5 corresponds to the surface plasmon resonance supported by the periodic array, which can be understood as a plasmonic standing wave on the surface of the antenna array. The more pronounced dip at shorter wavelengths around 406 nm with Q-factor of ~ 10.5 corresponds to a plasmonic standing wave localized inside the apertures, which is not strongly affected by changes in the upper or SiO_2 layers [13].

Highlight - 2nd REVISION

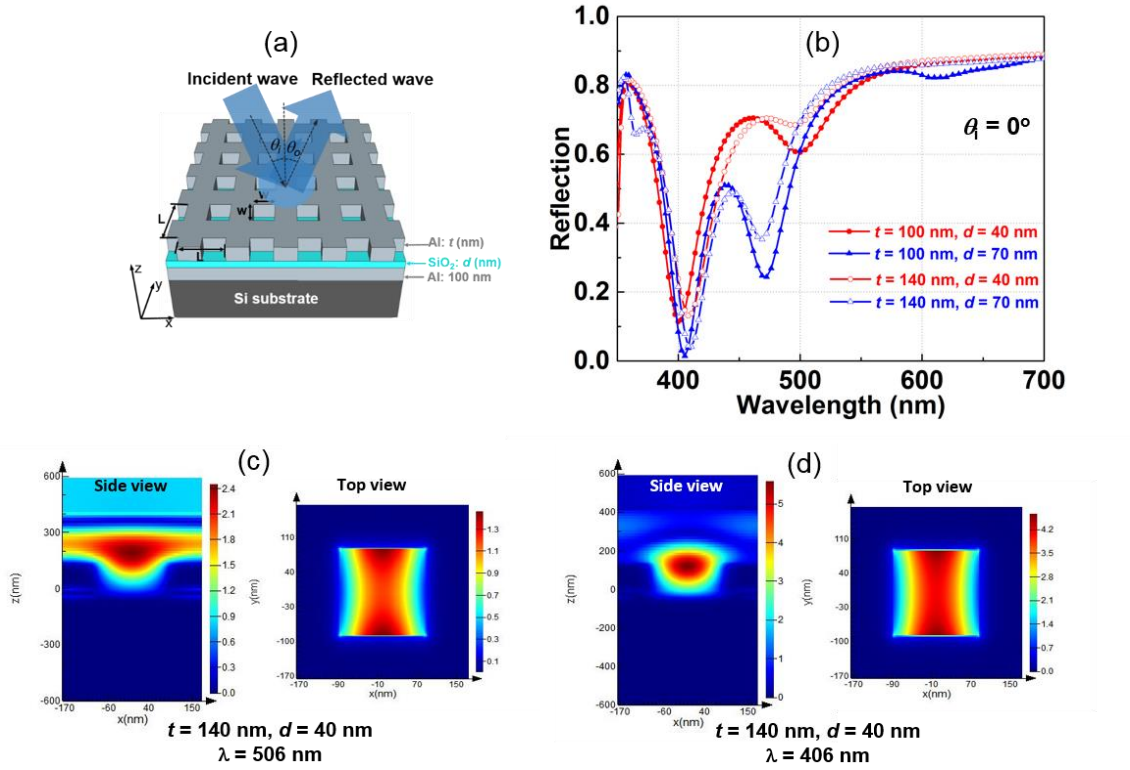

Fig. 1. (a) The designed MDM antenna structure. (b) The reflection spectra for several aluminium (t) and silica (d) thicknesses. (c) and (d) show the electric field distributions at side- and top-views at the longer and shorter resonances of λ = 506 nm and λ = 406 nm, respectively. The parameters of antenna structure of t = 140 nm and d = 40 nm are chosen for the results in Figs. 1(c) and 1(d).

These resonant characteristics can be seen in Figs. 1(c) and 1(d) which show the electric field distributions in side and top view at the two resonances. Fig. 1(c) shows the distributed nature of the longer wavelength resonance and Fig 1(d) shows the strong localisation for the shorter wavelength resonance. Both of these may be useful for different types of sensing applications.

To understand the angular dependence on the optical properties, we have next calculated the reflectance of the structure versus the incident angle. This also relates to the type of optical characterisation that will be carried out later in the paper. The oblique incident angle θ_i is defined by the angle between wavevector k and the z axis. An inter-layer SiO_2 of 40nm and upper Al thicknesses of 140 nm are chosen for the simulation. The structure is not sensitive to polarization due to its symmetry in x and y directions, so that only dependence of the reflectance spectrum on the incident angle θ_i for electric polarization along x direction is shown in Fig. 2. The blue shaded region around 400 nm in these figures represent a decrease in reflectance and hence indicates the presence of a strong optical mode. This resonance remains for a wide range of angles, which could be useful in a number of sensing applications in fluorescence based biosensing.

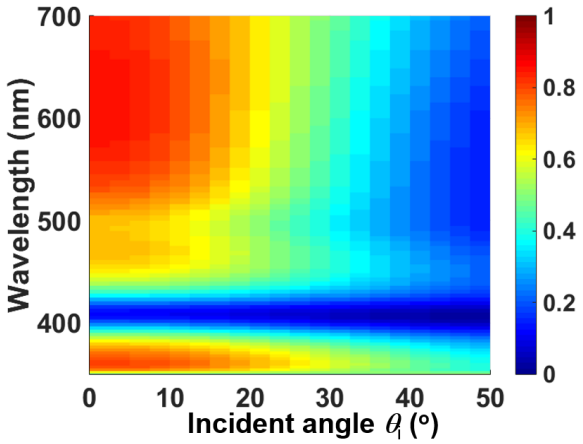

Fig. 2. Simulated oblique angle dependence on the reflection spectra of the nanoantenna structure depicted in Fig. 1(a) for t = 140 nm and d = 40 nm for x polarization.

B. Sample preparation and characterization

The Al-SiO_2-Al structure was fabricated on a 24 mm x 24 mm x 1 mm silicon (100) substrate. The lower Al layer was deposited by sputter coating (Leybold L560) at a fixed deposition rate of 2 Å/s. An ultra-thin chromium (Cr) layer (~5 nm) was used as an intermediate layer to improve Al adhesion [15]. Then, the SiO_2 buffer-layer was deposited using Plasma Enhanced Chemical Vapour Deposition (PECVD) and finally, the upper Al layer was deposited by sputter coating (Leybold L560) at a fixed deposition rate of 2 Å/s. The second step was patterning of antenna arrays using the focused-ion-beam (FIB). The FIB current and dwell time are the main parameters that effect the etching width and depth for a fabricated antenna arrays. Fig. 3 (a) shows a cross-section of this tri-layer structure viewed after FIB cross-sectioning. A thin layer of platinum (Pt) has been deposited over the upper Al layer to aid the imaging and cross-sectioning process. A dark SiO_2 layer can be seen between the two Al layers. The thicknesses of the layers were measured as: upper Al ~ 140 nm, SiO_2 ~ 40 nm, and lower Al ~ 100 nm. The thickness of upper Al layer is larger than expected thickness of 100 nm, but this does not greatly influence the optical properties of the antenna arrays. Fig. 3(b) shows the surface of the ~5 x 5 μm^2 antenna arrays, the average period is 350 nm and square size is 175 nm x 175nm.

The reflectance (*R*) measurements of the nanoantenna arrays were carried out by Fourier spectroscopy. The wide angular reflected light was collected from a 5 x 5 μm^2 focusing area using an objective with a high numerical aperture (Zeiss EPIPLAN 100X NA = 0.8). In order to measure reflectance from a device we first measure a background reference reflectance from an Al mirror. The Fourier microscope uses a spectrometer (Ocean Optics USB 2000+) for the far UV and visible parts of the spectrum and the results shown here have some noise in the UV range due to the detector and the limited transmission of the optics in this range. Fig. 4(a) shows the reflectance colour map of the fabricated sample depicted in Fig. 3 for *y* electric field polarization. As can be seen in Fig. 4(a), the resonance at around 400 nm can be observed along with a broader -shallower resonance around 530nm. The comparison between the measured and simulated results at normal incidence is shown in Fig. 4(b) and reasonable

level of agreement is obtained, considering the fabrication imperfections which will be present in the measured structure. Also the finite size of the measured sample will cause some discrepancies.

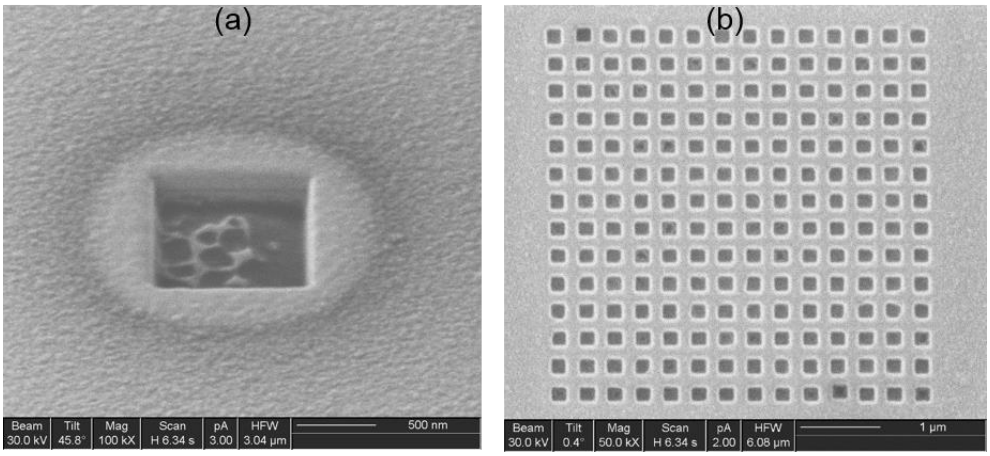

Fig. 3. SEM image of the nanoantenna array made by subwavelength aperture arrays having period of 350 nm and side length of 175 nm in Al-SiO_2-Al structure. (a) a FIB cross-section and (b) top-view.

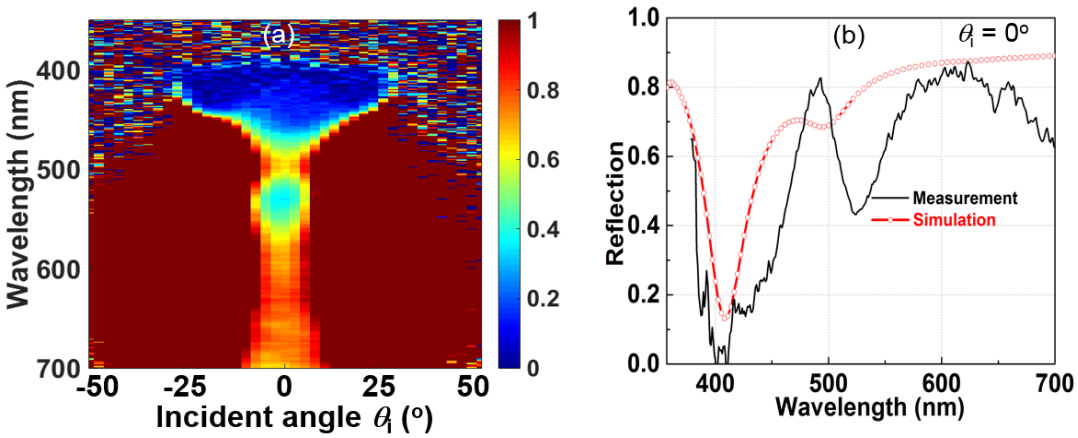

Fig. 4. (a) Reflectance colour map for 5x5 μm^2 MDM antenna arrays shown in Fig. 3 for x polarization, measured using Fourier spectroscopy; (b) The quantitative comparison between measured and simulated reflection spectra at normal incidence for x polarization. The parameters of antenna structure of t = 140 nm and d = 40 nm are chosen for simulation.

3. RESULTS AND DISCUSSION

In order to model the fluorescence emission enhancement produced by the MDM antenna arrays shown in Fig. 1(a), we simulated the interaction of an electric dipole source with the MDM antenna arrays. In order to simplify the analysis an E_y electric dipole is positioned at the middle of the upper Al layer. We plotted the power enhancement with the electric dipole source 15 nm away from the surface aperture as depicted in inset of Fig. 5(a) showing a single unit cell. The enhancement is the total power through a plane 50 nm above the upper surface normalised to the power that would have been emitted through the plane by the source in free space. The infinite antenna arrays

are simulated by using periodic boundary conditions in the lateral directions. As Fig. 5(a) shows, in the case of the MDM antenna arrays, we obtain asymmetric type resonances with enhancements of 5.2 times at 406 nm and 1.5 times at 506 nm. The enhancement peaks correspond to the two resonances shown in Fig. 1(b). The enhancement of a MDM single element is also calculated and shows lower enhancement and are blue-shifted to 2.85 times at 370 nm in Fig. 5 (a). The narrow enhancement spectrum of MDM antenna arrays compared with the MDM single cell is due to the coupling between the antenna elements [10]. As can see in Fig. 5(a), the very low intensity enhancement of the longer wavelength at around 506 nm compared to the shorter wavelength at around 406 nm is because of larger mode volume seen in Fig. 1(c) and small *Q*-factor resulting in lower Purcell factor [30,31]. Fig. 5(b) shows the transverse cross-section through the far-field radiation patterns at the resonant peaks shown in Fig. 5(a). In the measurement, the laser spot illuminates an area of 2 x 2 μm^2, based on the antenna periodicity, this covers a roughly 6 x 6 portion of the array and this size of array is used in the far field calculation. The emission has a symmetric pattern in x-z plane with an emission maximum at normal and high directivity emission with a Full Width Half Maximum (FWHM) beamwidth of 8.34 deg. As expected there is a wide emission angle with a FWHM beamwidth of 106.2 deg at normal for the MDM single cell. The narrow emission peak for the MDM antenna array results from the strong inter-element coupling and focusing effects in the MDM antenna array [10].

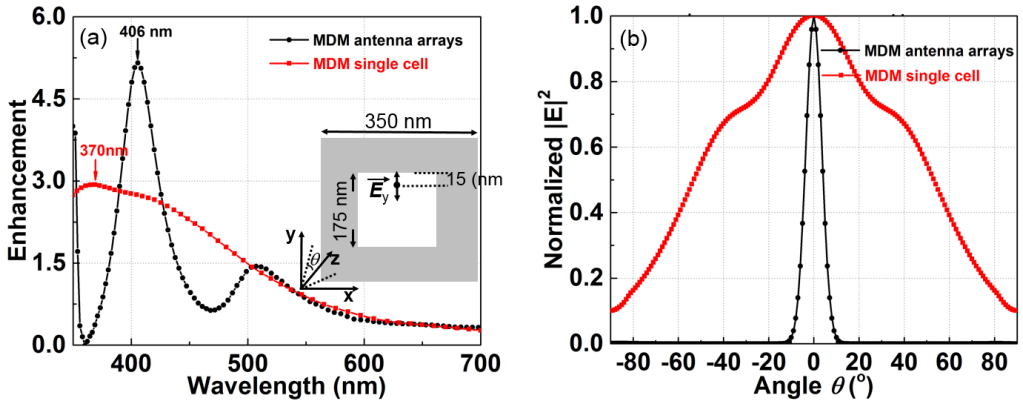

Fig. 5. (a) Simulated electric field intensity enhancements for several antenna structures: MDM antenna arrays (dotted-solid-black curve) and MDM single cell (square-solid-red curve). (b) Transverse sections through far field radiation pattern of 6x6 subset of infinite array antenna for x-z plane at the wavelenths noted in (a). Each radiation pattern has been normalized to its respective maximum.

Highlight - 2nd REVISION

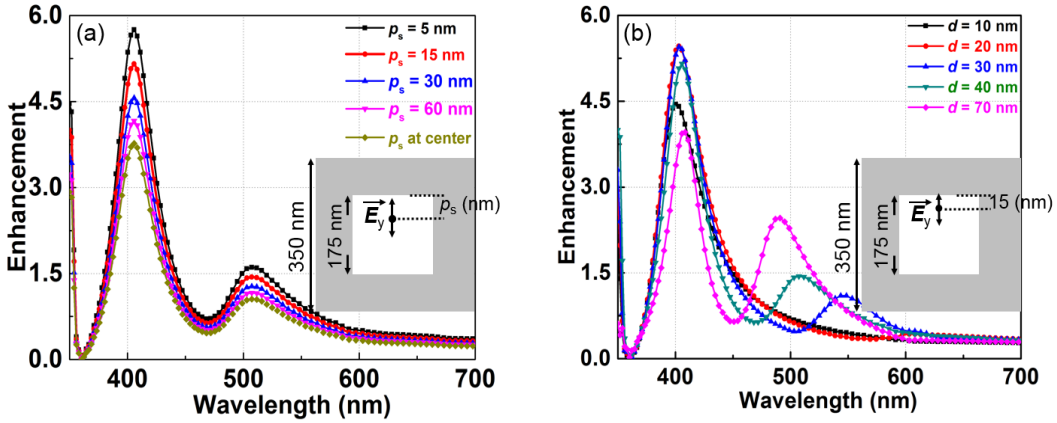

Fig. 6. Intensity enhancement for (a) Several positions of dipole source within the aperture and (b) a number of SiO_2 layer thicknesses.

The intensity enhancement of a MDM dipole nanoantenna is determined by a number of parameters, here the effect of varying dipole position, SiO_2 gap size, and the aperture shape and size are presented. Firstly, in Fig. 6(a) the position of dipole source p_s, has been moved away from the edge of the aperture, starting at 5 nm to the centre of aperture hole at 87.5 nm. Other parameters were kept as, d = 140 nm, t = 40 nm, L = 350 nm, and w = 175 nm for all simulations. The enhancement spectra show a number of interesting trends. The LSPR wavelength does not change and the intensity enhancement reduces by 34% as the dipole moves from the edge to the centre (5.8 times to 3.8 times). For example, we obtain the field enhancement peaks of 5.2 times and 4.6 times at 406 nm for the dipole sources p_s of 15 nm and 30 nm, respectively. Next, the effect of varying the silica gap thickness is observed, this is an important variable as it controls the reflectance and the amount of intensity enhancement in the gap with smaller gaps giving larger enhancement around 400 nm. The position of dipole source at 15 nm from the metallic surface remains constant, Fig. 6(b) shows the results of the varied gap size for several thicknesses of 10 nm, 20 nm, 30 nm, 40 nm, and 70 nm, the resonant wavelength near 400 nm remains stationary and the enhancement is maximum at around 5.5 times with a FWHM of around 42 nm for the silica gap thickness at around 30 nm ~ 40 nm. The longer resonance near 500 nm is blue-shifted and increases in enhancement for increasing the silica thickness.

Highlight - 2nd REVISION

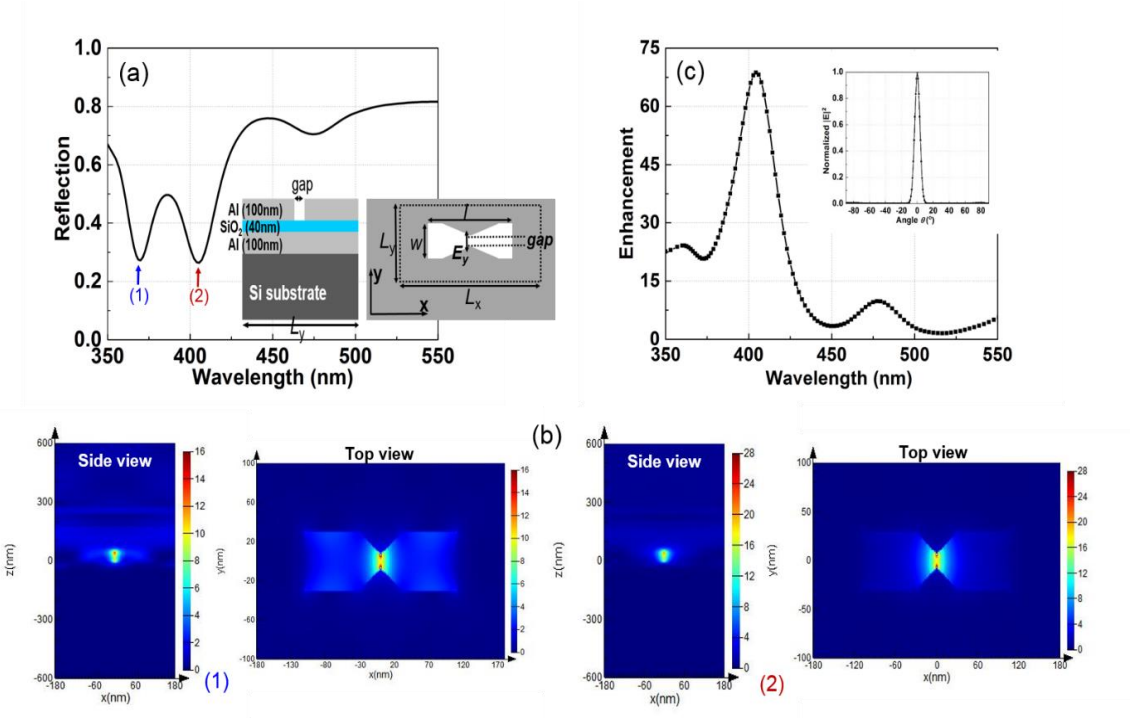

Fig. 7. (a) Inset: Designed nanoantenna arrays based on inverted bowtie shape arrays in MDM structures for L_x = 360 nm, L_y = 200 nm, w = 60 nm, l = 220 nm, and gap = 15 nm; main figure shows the reflectance spectrum of the inverted bowtie shape arrays in MDM structure depicted in inset for normally incident wave and electric field along to the y axis (E_y); (b) electric field profiles along to the y axis (side view) and z axis (top view) at two resonances are also noted in Fig. 7(a); (c) the normalized intensity enhancement at the plane 50 nm above the upper antenna surface for the E_y dipole source located at the middle of the gap. The normalized radiation pattern of the resonance at around 404 nm is noted in the inset of Fig. 7(c).

Recently, bowtie nanoantenna arrays in the MDM configuration have been designed for refractive index sensing application for the operating wavelength from 800 nm to 1,500 nm [32]. Here we show strong field enhancement by using inverted aperture type bowtie nanoantenna arrays in a MDM configuration. The bowtie aperture shape perforates the top aluminium layer as shown in the inset of Fig. 7(a). The rectangular lattices are L_x and L_y of 360 nm and 200 nm, respectively. The bowtie parameters of w = 60 nm, l = 220 nm, and the gap = 15 nm are chosen for simulation. The reflectance spectra depends on polarization, and for y polarization the reflectance spectrum for normal incidence is shown in Fig. 7(a). As seen in Fig. 7(a), two main resonant peaks at 369 nm and 404 nm corresponding to *Q*-factors of around 10.5 and 12.5, are observed in the range from 350 nm to 550 nm. The electric field profiles in side and top view at these resonances are shown in Fig. 7(b). Looking at the electric field profiles in Fig. 7(b), the first (at 369 nm) and second (at 404 nm) resonances show the similar profiles, but the first resonance at 369 nm shows lower amplitude compared to the second, so it will show smaller electric field intensity enhancement when an E_y dipole source is applied at the centre of the gap.

Figure 7(c) shows the simulated results of the field intensity enhancement and far-field radiation pattern of 6x6 subset (in the inset) of the antenna structure depicted in inset of Fig. 7(a) for a E_y dipole source located at the middle of the gap. As can be seen, the field intensity enhancement can be up to 67 times at around 404 nm with a FWHM alongside centre peak wavelength of 31.1 nm. We also see the high directivity emission with small beamwidth of ~15 deg as shown in inset of Fig. 7(c). These results are very promising for sensing applications, even though FIB etching of these structures will be challenging, techniques such as electron beam lithography and nanoimprint lithography are able to produce larger arrays of such structures.

4. CONCLUSIONS

We have presented and investigated subwavelength nanoantenna aperture arrays in metal-dielectric-metal structures which produce significant intensity enhancement and highly directive emission. The silica layer sandwiched between two metallic layers plays an important role to enhance the antenna efficiency and it needs to be optimized for maximum efficiency. These aperture based arrays, will be very suitable for sensing applications where the apertures will tend to hold any analyte in the high field regions. In addition, we have proposed an aperture bowtie nanoantenna in the metal-dielectric-metal configuration which combines very high enhancement of up to 67 times and highly directivity emission with a beamwidth of ~15 deg.

Acknowledgement. The authors acknowledge funding from the UK Newton Research Collaboration Program and Dr. Duncan Allsopp and Dr. Philip Shields of the University of Bath, and Dr. Andy Murray of the University of Bristol for assistance in structure fabrication.

References

1. H. A. Atwater, “The promise of plasmonics,” Scientific American **296**, 56 (2007).

2. E. Ozbay, “Plasmonics: merging photonics and electronics at nanoscale dimensions,” Science **311**, 189-193 (2006).

3. S. A. Maier, Plasmonics: Fundamentals and applications (Springer, 2007).

4. A. Tittl, H. Giessen, and N. Liu, “Plasmonic gas and chemical sensing,” Nanophotonics **3**, 157 (2014).

5. J. N. Anker, W. P. Hall, O. Lyandres, N. C. Shah, J. Zhao, and R. P. Van Duyne, “Biosensing with plasmonic nanosensors,” Nature Materials **7**, 422 (2008).

6. H. Jans and Q. Huo, “Gold nanoparticle-enabled biological and chemical detection and analysis,” Chem. Soc. Rev. **41**, 2849 (2012).

7. T. Chung, S. -Y. Lee, E. Y. Song, H. Chun, and B. Lee, “Plasmonic nanostructures for nano-scale bio-sensing,” Sensors **11**, 10907 (2011).

8. V. J. Sorger, R. F. Oulton, R. -M. Ma, and X. Zhang, “Toward integrated plasmonic circuits,” MRS bulletin **37**, 728 (2012).

9. Z. Skeete, H. -W. Cheng, Q. M. Ngo, C. Salazar, W. Sun, J. Luo, and C. -J. Zhong, "'Squeezed' interparticle properties for plasmonic coupling and SERS characteristics of duplex DNA conjugated/linked gold nanoparticles of homo/hetero-sizes," Nanotechnology **27**, 325706 (2016).

10. N. Dorh, A. Sarua, J. Stokes, N. A. Hueting, and M. J. Cryan, "Fluorescent emission enhancement by aluminium nanoantenna arrays in the near UV," J. Optics **18**, 075008 (2016).

11. J. L. Stokes, Y. Yu, Z. H. Yuan, J. R. Pugh, M. Lopez-Garcia, N. Ahmad, and M. J. Cryan, "Analysis and design of a cross dipole nanoantenna for fluorescence-sensing applications," J. Opt. Soc. Am. B **31**, 302 (2014).

12. R. J. Veenkamp and W. N. Ye, "Plasmonic metal nanocubes for broadband light absorption enhancement in thin-film a-si solar cells," J. Appl. Phys. **115**, 124317 (2014).

13. T. J. Seok, A. Jamshidi, M. Kim, S. Dhuey, A. Lakhani, H. Choo, P. J. Schuck, S. Cabrini, A. M. Schwartzberg, J. Bokor, E. Yablonovitch, and M. C. Wu, "Radiation engineering of optical antennas for maximum field enhancement," Nano Lett. **11**, 2606 (2011).

14. R. Fernández-García, Y. Sonnefraud, A. I. Fernández-Domínguez, V. Giannini, and S. A. Maier, "Design considerations for near-field enhancement in optical antennas," Contemporary Physics **55**, 1 (2014).

15. D. Wang, W. Zhu, Y. Chu, K. B. Crozier, "High directivity optical antenna substrates for surface enhanced Raman scattering," Adv. Mater. **24**, 4376 (2012).

16. R. Fernandez-Garcia, M. Rahmani, M. Hong, S.A. Maier, and Y. Sonnefraud, "Use of a gold reflecting-layer in optical antenna substrates for increase of photoluminescence enhancement," Opt. Express **21**, 12552 (2013).

17. A. W. Powell, D. M. Coles, R. A. Taylor, A. A. R. Watt, H. E. Assender, and J. M. Smith, "Plasmonic gas sensing using nanocube patch antennas," Adv. Opt. Mater. **4**, 634 (2016).

18. P. K. Jain, X. Huang, I. H. El-Sayed, M. A. El-Sayed, "Review of some interesting surface plasmon resonance-enhanced properties of noble metal nanoparticles and their applications to biosystems," Plasmonics **2**,107 (2007).

19. R. Bardhan, W. Chen, C. Perez-Torres, M. Bartels, R. M. Huschka, L. L. Zhao, E. Morosan, R. G. Pautler, A. Joshi, and N. J. Halas, "Nanoshells with targeted simultaneous enhancement of magnetic and optical imaging and photothermal therapeutic response," Adv. Funct. Mater. **19**, 3901 (2009).

20. T. W. Ebbesen, H. J. Lezec, H. F. Ghaemi, T. Thio, and P. A. Wolff, "Extraordinary optical transmission through subwavelength hole arrays," Nature **391**, 667 (1998).

21. L. Martin-Moreno, F. J. Garcia-Vidal, H. J. Lezec, K. M. Pellerin, T. Thio, J. B. Pendry, and T. W. Ebbesen, "Theory of extraordinary optical transmission through subwavelength hole arrays," Phys. Rev. Lett. **86**, 1114 (2001).

22. A. G. Brolo, R. Gordon, B. Leathem, and K. L. Kavanagh, "Surface plasmon sensor based on the enhanced light transmission through arrays of nanoholes in gold films," Langmuir **20**, 4813 (2004).

23. A. De Leebeeck, L. K. S. Kumar, V. de Lange, D. Sinton, R. Gordon, and A. G. Brolo, "On-chip surface based detection with nanohole arrays," Anal. Chem. **79**, 4094 (2007).

Highlight - 2nd REVISION

24. A. Lesuffleur, H. Im, N. C. Lindquist, K. S. Lim, and S. -H. Oh, “Laser-illuminated nanohole arrays for multiplex plasmonic microarray sensing,” Opt. Express **16**, 219 (2008).

25. A. Kinkhabwala, Z. Yu, S. Fan, Y. Avlasevich, K. Müllen, and W. E. Moerner, “Large single-molecule fluorescence enhancements produced by a bowtie nanoantenna,” Nat. Photonics **3**, 654 (2009).

26. H. Aouani, O. Mahboub, N. Bonod, E. Devaux, E. Popov, H. Rigneault, T. W. Ebbesen, and J. Wenger, “Bright unidirectional fluorescence emission of molecules in a nanoaperture with plasmonic corrugations,” Nano Lett. **11**, 637 (2011).

27. A. G. Curto, G. Volpe, T. H. Taminiau, M. P. Kreuzer, R. Quidant, and N. F. van Hulst, “Unidirectional emission of a quantum dot coupled to a nanoantenna,” Science **329**, 930 (2010).

28. Lumerical FDTD Solutions (Lumerical Solutions, Inc.). https://www.lumerical.com/

29. A. Taflove, Computational electrodynamics (Artech House, Boston, 1995).

30. E. M. Purcell, “Spontaneous emission probabilities at radio frequencies,” Proc. Am. Phys. Soc. **69**, 681 (1946).

31. A. F. Koenderink, “On the use of Purcell factors for plasmon antennas,” Opt. Lett. **35**, 4208 (2010).

32. L. Lin and Y. Zheng, “Optimizing plasmonic nanoantennas via coordinated multiple coupling,” Sci. Rep. **5**, 14788 (2015).